CARBON 91 (2015) 266–274

Available at www.sciencedirect.com

ScienceDirect

journal homepage: www.elsevier.com/locate/carbon

Under pressure: Control of strain, phonons and bandgap opening in rippled graphene

U. Monteverde [a], J. Pal [a], M.A. Migliorato [a,*], M. Missous [a], U. Bangert [b], R. Zan [e], R. Kashtiban [c], D. Powell [d,1]

[a] School of Electrical and Electronic Engineering, University of Manchester, UK
[b] Department of Physics and Energy, University of Limerick, Ireland
[c] Department of Physics, University of Warwick, UK
[d] Albourne Partners (Cyprus) Ltd, Cyprus
[e] Department of Physics, Faculty of Arts and Sciences, Niğde University, Turkey

ARTICLE INFO

Article history:
Received 5 February 2015
Accepted 15 April 2015
Available online 23 April 2015

ABSTRACT

Two-dimensional (2D) layers like graphene are subject to long-wavelength fluctuations that manifest themselves as strong height fluctuations (ripples). In order to control the ripples, their relationship with external strain needs to be established. We therefore perform molecular dynamics (MD) of suspended graphene, by the use of a newly developed force field model (MMP) that we prove to be extremely accurate for both C Diamond and Graphene. The MMP potential successfully reproduces the energy of the σ-bonds in both sp^3 and sp^2 configuration. Our MD simulations and experimental electron microscopy analysis reveal that ordered and static ripples form spontaneously as a direct response to external pressure. Furthermore the morphology of graphene and strain response of the crystal bonds differ depending on the particular directions where external pressure is present. Different regions of the strained graphene sheet are then investigated by tight-binding. Localised bandgap opening is reported for specific strain combinations, which also results in particular signatures in the phonon spectrum. Such controllable morphological changes can therefore provide a means to practically control and tune the electronic and transport properties of graphene for applications as optoelectronic and nanoelectromechanical devices.

1. Introduction

For many years the atomistic empirical potential treatment in molecular dynamics (MD) has provided the only viable alternative to computationally expensive *ab initio* methods [1]. Though many empirical methods [2–5] were initially developed for 3D bulk semiconductor crystals, in recent years much work has gone into generating force fields [6–11] capable of accurately describing the essential features of nanostructures and 2D crystal structures such as graphene [12].

Graphene is experimentally observed to exhibit height variations (ripples) [13–15] in response to external

* *Corresponding author.*
E-mail address: max.migliorato@manchester.ac.uk (M.A. Migliorato).

[1] Any work contributed to this paper by Dr. Dave Powell was in his personal capacity. The findings and any opinions expressed in this publication are the authors' own and do not reflect the view of Albourne Partners (Cyprus) Ltd.

http://dx.doi.org/10.1016/j.carbon.2015.04.044
0008-6223/

perturbations. Such perturbations can be caused by long range fluctuations [13], impurities adhering to the surface [16] or interaction with the substrate [17] and it affects the physical characteristics of graphene [18–20]. Therefore the study of the morphology of graphene sheets under non idealised conditions and its impact on vibrational properties, electronic structure and transport characteristics can provide useful and practical strategies to create bespoke functionalities [21,22]. It has been suggested that by reversing the strain–ripple formation relationship, vibrational or pressure sensors can be engineered [23].

In order to reveal the strain–ripple formation mechanism, in this work we use MD simulations with a recently proposed interatomic many-body empirical potential (MMP potential) [24,25] which has been extensively tested for Group IV Silicon and Germanium semiconductors. The MMP potential overcomes the classic shortcomings observed [3,26] in short range pair potentials, i.e. the impossibility of obtaining a satisfactory representation of elastic and vibrational properties with a single set of parameters. This adversely impacts on the ability to model thermodynamic properties such as the coefficient of thermal expansion.

In this work we continue using the MMP for carbon based crystals. Further to satisfying the criteria of correctly and simultaneously predicting vibrational and elastic properties of diamond, we will illustrate how the same parameter set is also able to correctly predict the essential features of other crystal phases such as graphene.

The MMP potential is used here to predict ripple formation in suspended graphene sheets. We will show how two types of ripples form in response to strain. The first is a wave front ripple orthogonal to the strain front if external strain is applied along a single direction. The second is a sinusoidal shape which emerges if the external strain is applied simultaneously along two orthogonal directions. In both cases ripples form in order to relax the external strain, although ripples are never fully relaxed and in fact exhibit a different strain component (shear) to the ones externally applied, together with internal relaxation i.e. breaking of the hexagonal symmetry into two sublattices. Such types of strain are useful as they result in modification of the bandgap around the Dirac point, where unstrained graphene exhibits a zero bandgap and is therefore metallic in nature. When ripples form instead, we show that Tight Binding calculations predict a significant bandgap opening in the proximity of the Dirac point, where graphene would thus exhibit semiconducting rather than its usual metallic behaviour. We have also analysed the vibrational spectrum in the semiconducting regions and we report that particular signatures in the measured phonons can be uniquely associated with the presence of a bandgap.

2. Modelling

2.1. C-Diamond

Compared to the other commonly used semiconductor materials of group IV, tetrahedrally bonded C-Diamond has distinctive mechanical properties: a small lattice constant, a very large negative cohesive energy and large elastic moduli [27]. Furthermore the large elastic constants, which are due to the very strong carbon–carbon dimer bonds, are also indicative of a strong tendency to resist any crystal distortions. Using a large data set of mechanical and vibrational properties we have obtained a parameter set for the MMP potential.

For a detailed comparison between other measured/calculated mechanical properties, phonon frequencies, Grüneisen parameters of C-Diamond (together with a comparison between different crystal phases) and the MMP simulated values see Tables S1–S4 in Supplementary Material (SM).

The calculated vibrational spectrum of diamond is given in Fig. 1(A) and is compared to experimental data. The dispersion curves of diamond have distinct characteristics when compared to the other sp^3 bonded materials. For instance the Transverse Acoustic (TA) phonons do not present the characteristic flat band in the proximity of the X point of the Brillouin zone, which is present in both Si and Ge and is usually assumed to originate from long range forces. A further feature of the phonon spectrum is the experimentally observed [28–31] and theoretically predicted [32] "overbending" of the Longitudinal Optical (LO) branches, e.g. a maximum of the dispersion between the Γ and X points. The LO overbending, not observed in other group IV materials, is a signature of the importance of long range forces between second nearest neighbours (nn'') in describing the crystal dynamics [31]. The nn'' interactions, even if only partially included in the MMP potential, are sufficient to correctly reproduce both the LO overbending in all three directions of the wave vector, the parabolicity of the TA at the high symmetry point X and the large splitting between the LO and TO phonons between the Γ and X points, as shown in Fig. 1(A).

Other potentials [4–7] have been proposed that consider interactions up to the fifth neighbours. However, even with such long range forces, overbending and parabolicity are still incorrectly reproduced and the LO/TO splitting is absent.

2.2. Graphene

We have used the MMP potential (with exactly the same parameters of the diamond phase) to evaluate the structural and vibrational properties of graphene (see Tables S5 and S6 in SM). The measured phonon dispersion of graphene (Fig. 1(B)) is very similar to that of graphite, where two or more graphene planes are weakly interacting. Hence, the main difference between the phonon spectra arises from the out-of-plane vibrations. Near the central Γ point of the Brillouin zone, the out-of-plane acoustic modes (ZA) of graphite exhibit a distinct split which is not present in graphene. In Fig. 1(B) we compare the experimental and simulated (using the MMP potential) data. Overall the simulated curves match the measurements very well, though the characteristic overbending optical branches is not as well reproduced as in diamond. However the split between LO and TO near the Γ point is evident. Such a difference in phonon frequencies is not observed when using other empirical potentials [6,7]. The out-of-plane branches, ZA and ZO, are all in excellent agreement with the experimental data. For a comparison of the vibrational spectrum of graphene predicted by the MMP

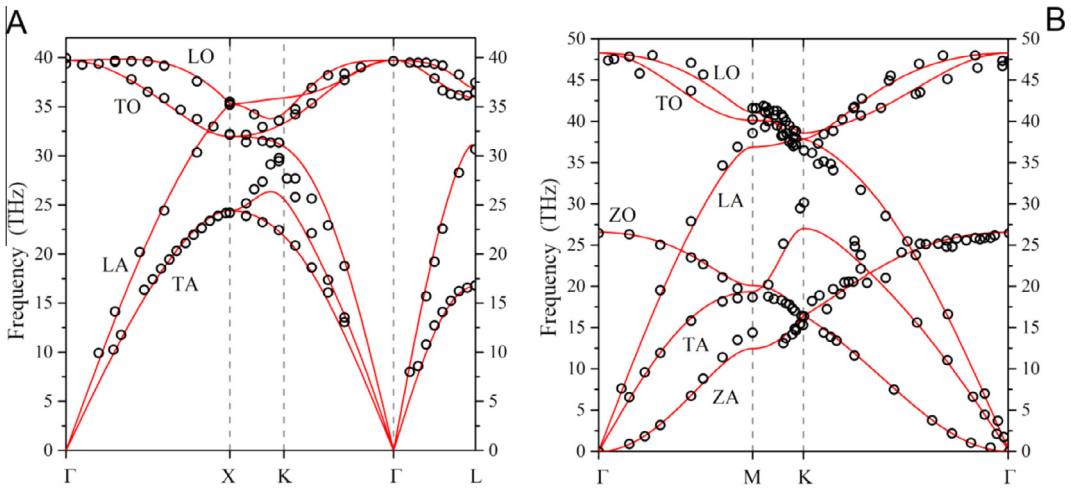

Fig. 1 – Predicted phonon dispersion curves. (A) C-Diamond and (B) Graphene calculated with the MMP potential. Experimental data are represented by open circles in C-Diamond [28–31] and Graphene [33,34]. The MMP potential, with a single set of parameters fitted to the C-Diamond phase also accurately reproduces the vibrational spectrum of 2D Graphene, indicating that π-bonding, which is not included in the MMP separately form σ-bonding, is sufficiently well described in the force field equations. (A colour version of this figure can be viewed online.)

potential and the most commonly used empirical models (LCBOPII [11], Lindsay-Broido [9], AIREBO [5]) see Fig. S1 in SM.

2.2.1. *Ripple formation in graphene*

Using MD we investigated ripple formation of the graphene sheet under different strain conditions to include tensile and compressive pressures. We considered both hydrostatic strain and along the ZigZag/Armchair directions, to which we will refer respectively as *x* and *y* since such is the alignment of our model structure in respect of the Cartesian axes.

The MD simulations, comprising around 4000 atoms, start from an atomically flat single graphene sheet. Pressure is simulated by rigidly displacing the atoms on the *xy* plane and taking the resulting increase/decrease of the simulation box into account. The initial structure is therefore a strained graphene sheet, energy minimisation then takes place (see Video V1 in SM) to relax the atomic structure. The initial small movement of the atoms is soon replaced by larger movements and ultimately a visible change in the morphology of the overall structure. Eventually ripples spontaneously form and exhibit a regular pattern.

In this work we concentrate on two types of strain. Firstly, compressive strain in the *x* direction of 3.5% together with tensile strain in the *y* direction of 3.5% (Fig. 2), and secondly, compressive strain of 3.5% in both the *x* and *y* directions (Fig. 3).

In the first case, static and wave front ripples orthogonal to the *x* direction are formed with around 5 Å height or depression for hills and troughs respectively. The expected wavelength of the ripples is around 10 nm (one ripple every 10 nm). In the second case a more complex morphology is observed. Ripples appear in a regular pattern, sinusoidal in nature, with fluctuation again of around 5 Å height or depression for hills and troughs respectively. The expected wavelength of the ripples is again around 10 nm. Such peculiar sinusoidal shape is a direct response to hydrostatic compressive pressure and can be thought of as resulting from two colliding wave fronts orthogonal to each other.

We have carried out simulations of several other graphene sheets of different dimensions (both larger and smaller) and the formation of ripples on a critical 10 nm wavelength results to be independent from the size of the structure. The morphology of the ripples (wavelength and heights) is strictly related to the initially induced stress.

Scanning Tunneling Microscopy imaging has reported ripples in suspended graphene with a characteristic V-shape which matches the result of our simulation [35], suggesting that hydrostatic pressure was present in the experimental sample. Similar ripple combinations have been recently reported in other studies [10,36,37], while other work suggests that ripples are an intrinsic feature of graphene [38,39].

2.2.2. *Strain*

We analysed the distortion of the atomic bonds on the ripples. In Figs. 2 and 3 bonds are coloured from red to blue to represent tensile to compressive strain, compared to the equilibrium bond length of a flat graphene sheet ($LC/\sqrt{3} = 1.43$ Å). Green indicates low (or zero) strain.

It is clear from the inset in Figs. 2 and 3 that a non-uniform strain distribution is predicted, the presence of which has been experimentally observed by Raman spectroscopy mapping of strain effects on a graphene sheet deposited on a flexible substrate [40]. Different other peculiar properties of graphene have been revealed by Raman spectroscopy, which has become an essential characterisation tool for investigating graphene [41].

We can explain the non-direct correspondence between ripples and stress with a loss of hexagonal symmetry in graphene, which produces the 2D equivalent of the Kleinman displacement for a 3D diamond structure (e.g. the rigid displacement of the two fcc sublattices with respect to each other in a diamond structure), a hypothesis already proposed by Davydov [42]. In the sp^3 tetrahedral bonding, when uniaxial

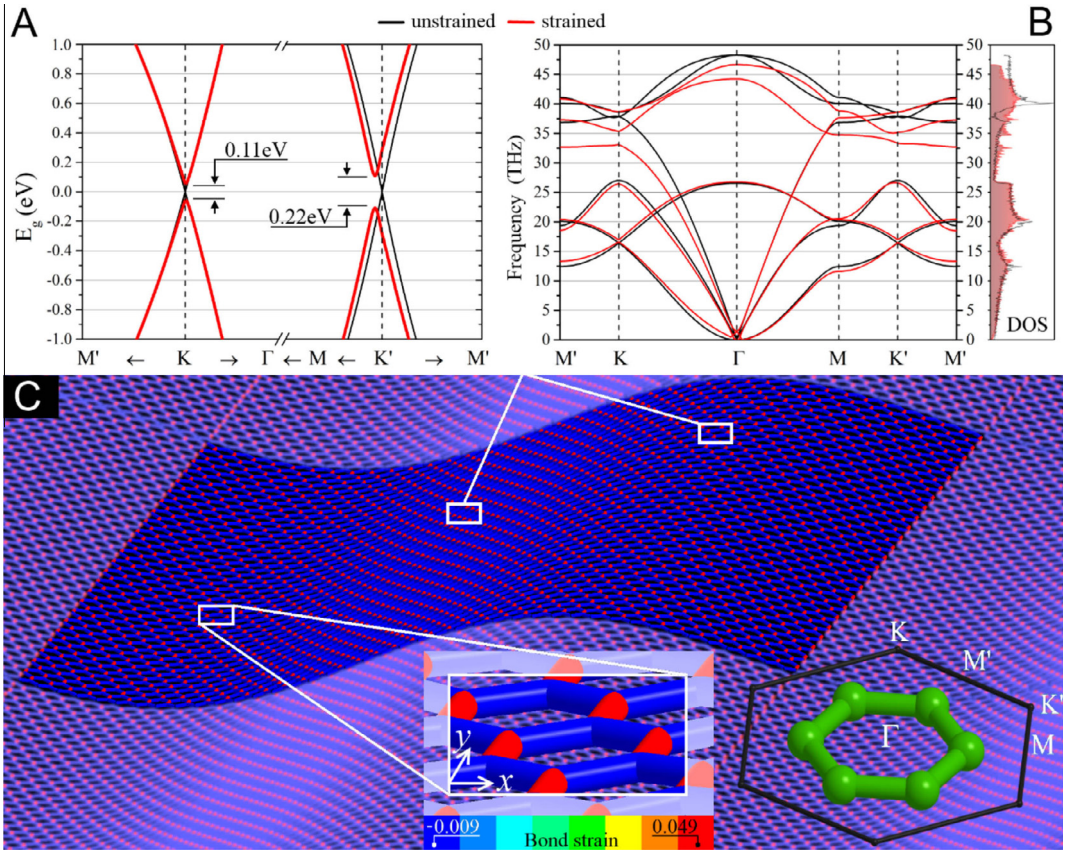

Fig. 2 – Free standing 10 × 10 nm graphene sheet with PBC under 3.5% compressive strain along x and 3.5% tensile strain along y. Colours in (C) indicate extended (red) or compressed (blue) bonds. The bandstructure (A) at the Dirac points, as calculated by tight binding, predicts a bandgap of 0.22 eV at the K′ point of the Brillouin zone. Non hydrostatic strain (e.g. shear or internal displacement) makes the K and K′, M and M′ points no longer degenerate. The phonon dispersion (B) is also substantially changed compared to the unstrained case. (A colour version of this figure can be viewed online.)

shear strain exists, the central atom relaxes causing the compression of one bond and the stretching of the other 3 bonds. What we observe in the insets of Figs. 2 and 3 is an equivalent behaviour for the sp^2 triangular bonding system. We have verified that such non uniformity is a function of the applied external pressure, albeit as a threshold activated process only for strains larger than 0.7 ± 0.1%. Based on experimental observations, Young et al. [43] suggested that the strain threshold is 0.6%, in excellent agreement with our model data. A further non intuitive observation is that while in the wave front ripple stretched and compressed bonds coexist throughout the sheet, strain switches from predominantly tensile to compressive along the ridge of the ripple (Fig. 3) which intuitively provides localised graphene areas (nanostructures) adjacent to each other but with very different strain and hence induced changes to the band structure as we will show in the following sections.

3. Electron microscopy

Experimentally ripples in suspended graphene can be indirectly observed by Electron Microscopy, which also allows to estimate their heights through focus changes in the high resolution electron microscopy (HREM) images. Furthermore, during the sample preparation for the microscopy (cleaning and transfer of the graphene sheet over holey grids, hydrocarbon contaminations, etc.) ripples can be involuntarily induced.

The non-flatness of the graphene sheet can be observed as colour differences in the HREM images. These can be related to physical heights which correspond to undulations with wavelengths of typically around 10 nm and amplitude up to 5 Å, identical to the height/depression predicted in our simulations (Figs. 2 and 3). In this way it is common to observe the wave front type ripples (see Fig. S2 in SM). However, this requires corrected scanning transmission electron microscopes with very small distances over which to achieve focus changes.

Another method is to apply a precise and narrow bandwidth filter to the Fast Fourier Transform (FFT) [44] (i.e. the computationally derived electron diffraction pattern) of a high resolution lattice image. In our case a ring filter corresponding to a width, in real space, of 0.002 Å was applied to high resolution electron microscopy phase contrast images obtained in a Jeol ARM200F transmission electron microscope. The filter radius was changed corresponding to fractions of Å, down to steps of 0.002 Å around the diffraction spot maxima. The shortening of the graphene a-lattice

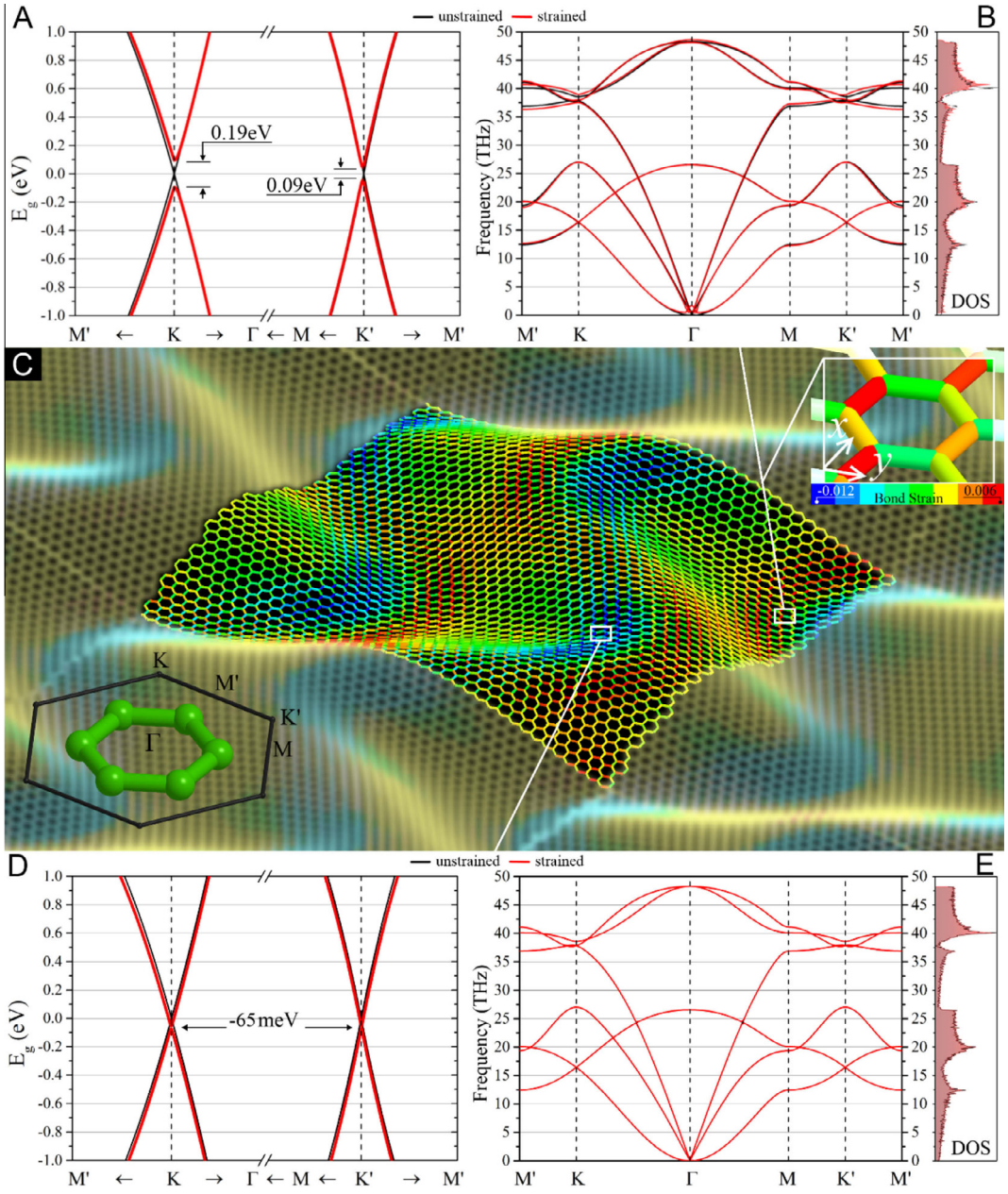

Fig. 3 – Free standing 10 × 10 nm graphene sheet with PBC under 3.5% hydrostatic compressive strain. Colours in (C) indicate extended (red) or compressed (blue) bonds. The bandstructure (A) at the Dirac points as calculated by tight binding predicts a bandgap of 0.19 eV at the K point of the Brillouin zone in the regions of tensile (red) strain. Non hydrostatic strain (e.g. shear or internal displacement) makes the K and K′, M and M′ points no longer degenerate. The phonon dispersion (B) is however not substantially changed compared to the unstrained case. Regions of compressive (blue) or low (to zero) strain (green) in (C) do not exhibit a bandgap (D) or changes in the phonon spectrum (E) compared to the unstrained case. However for compressive (blue) strain (D) the Dirac point lies below the Fermi energy by 65 meV thus exhibiting spontaneous n-doping behaviour. (A colour version of this figure can be viewed online.)

spacing (observed in-plane lattice constant) arising from lattice projections of undulated regions is of the order of 0.002–0.005 Å, so colour images in Fig. 4(C–J) represent top/bottom and flanks of undulations in focus. Note that the brighter colours (yellow/orange) indicate higher intensity in places where the chosen/filtered-out lattice spacing is most clearly seen in the images, whereas less pronounced intensity (blurring, blue hues) can be seen in places where the lattice spacings are not precisely congruent with the filter frequency. Note also that, in order to demonstrate the undulation effects, it is less important to identify the exact position of hills and troughs in the images, than to demonstrate the change in colour in a given location from yellow to blue with change of the corresponding filter frequency; this colour change is proof of the change in the projected lattice plane distance arising due to, in the Fig. 4, ripples of ~0.2 nm height/depth. Lattice

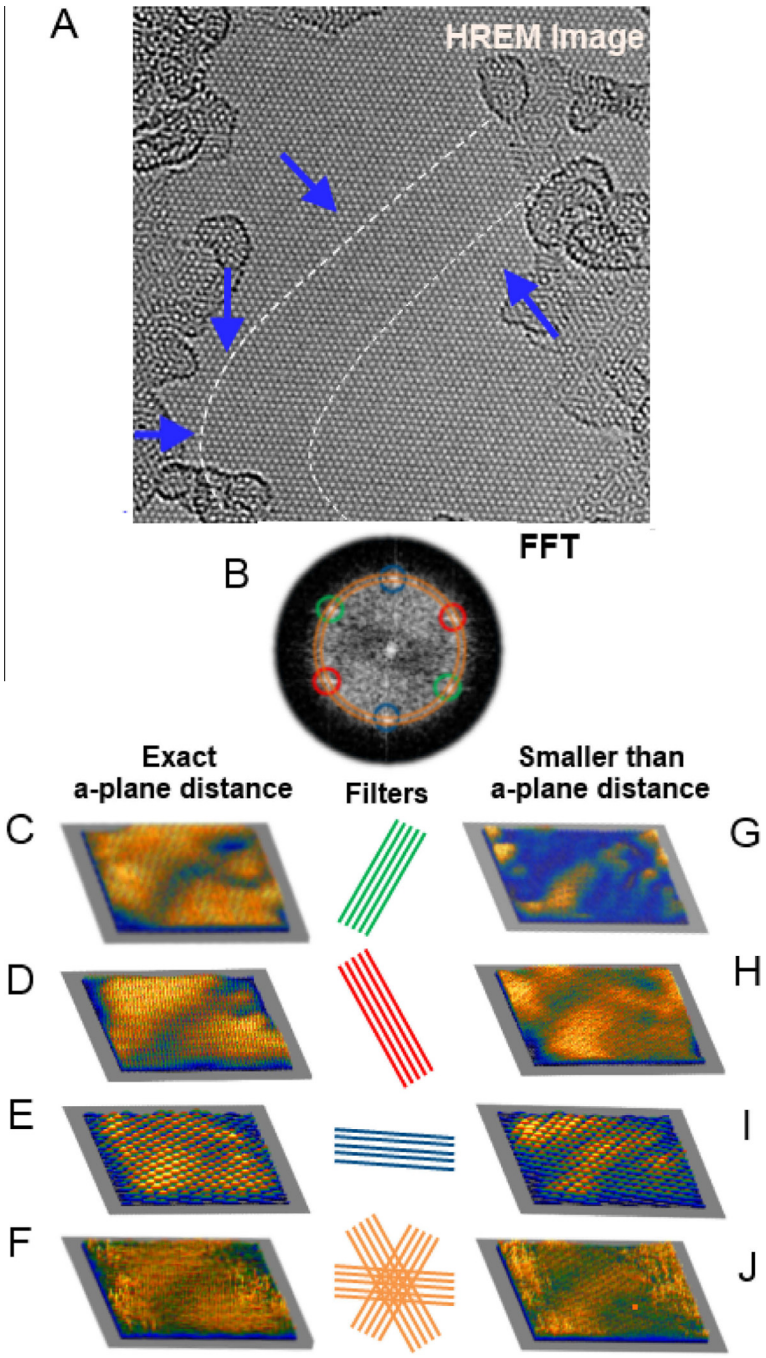

Fig. 4 – Electron Microscopy Images of a ripple surrounded by Hydrocarbon contamination. (A) HREM phase contrast image of single layer graphene obtained in a Jeol ARM 200F TEM. (B) FFT of the HREM image. (C–J) Inverse Fast Fourier Transform (IFFT) imaging with filters chosen to either match the exact a-plane spacing (unstrained, flat regions or regions under tension, (C–F)) or spacings smaller than those of the a-planes (unstrained, inclined regions or regions under compression, (G–J)). By comparing the orange regions in (C–J) one can assign the flanks of the hill (or trough) of the ripple. In (A) we also show the determined outline of the ripple and the presumed strain direction (blue arrows) originating from the hydrocarbon contamination. (A colour version of this figure can be viewed online.)

plane distances can also change due to compressive/tensile strain, and hence the overall effect has a twofold origin. However, it is possible, to a large extent, to identify and separate the two origins by studying IFFTs of individual sets of lattice planes as shown in Fig. 4. All lattice spacings of planes, which have directions with a component parallel to the ripple front will show some contraction at the ripple flank due to the projection. On the other hand, if regions where lattice planes cross a curved ripple front/flank perpendicularly show high filter passes (e.g. in Fig. 4(G)), this indicates compressive

strain. Also, if regions with lattice plane spacings larger than the a-plane spacing are detected, this implies tensile strain in these areas. Hence combining data of the filtered intensity and the direction in which the corresponding lattice planes cross the ripple front/flank can provide information, further to the mere existence and shape of ripples and their shape, about tension/compression within this shape.

Fig. 4(C–J) shows the hill, through and flank of a ripple, which is a mixture of wave front and sinusoidal type. The flank direction is indicated in the high resolution electron microscopy (HREM) image. This suggests, in accordance with our simulated results, that the hydrocarbon contaminants, visible in the micrograph as surface platelets, result in a uniaxial strain, in this case, predominantly in the (*xy*)-direction. The ripple is observed to curve at the bottom left of the image, which introduces tensile strain (bottom left of Fig. 4(E)) as well as compressive strain (bottom left of Fig. 4(G and H)) along the 'bend', again, in accordance with our strain calculation for the sinusoidal ripple (Fig. 3). The blue colouration along the wave front (straight) part in Fig. 4(C) and Fig. 4(G) as well as in the combined-effect image in Fig. 4(F), arises from the projection shortening of the inclined bonds. From this analysis one can conclude that both uniaxial strain and hydrostatic strain are introduced by the hydrocarbons and their respective directions can be inferred by the resulting shape of the ripples (blue arrows in Fig. 4(A)).

4. Bandstructure and vibrational spectrum

In Figs. 2 and 3 we show the tight binding calculated bandstructure in the proximity of the Dirac point for particular areas (unit cells) of the graphene sheet (for the entire Brillouin zone calculated bandstructure see Fig. S3 in SM). The red lines are compared to the unstrained case (black lines). Non hydrostatic strain (e.g. shear or internal displacement) introduces non equivalencies in the high symmetry points, so that the K and M points are no longer degenerate and both the band structure and phonon dispersions need to be described with the addition of the K′ and M′ points.

Significant shear strain induced bandgap opening has been both predicted [45,46], measured [47,48] and also deliberately introduced as result of patterned hydrogenation [49].

For both types of ripples the bandgap opens. The opening is of 0.22 eV (0.11 eV) near the K′ (K) point for the wave front ripple and 0.19 eV (0.09 eV) at the K (K′) point for the sinusoidal ripple, albeit in this case only in the regions with predominantly tensile strain. In the compressive strain regions the bandgap opening is negligible and the only difference compared to the unstrained case is that the Dirac point is found below the Fermi energy by 65 meV, thus exhibiting strain activated spontaneous n-doping characteristics.

Increasing the induced strain beyond 6% (we have performed simulations with different stress combinations, from 0.5% to 15% strain) of the suspended graphene sheet does not substantially affect the bandgap or the semiconducting regions. The 3.5% strain combinations represent a trade-off between bandgap opening and density of semiconducting regions, while matching as well with our TEM observations.

It is also noticeable that for the wave front ripple the phonon dispersion is very different compared to the unstrained case, with a distinct change in the density of states (DOS) for the optical phonon modes. This is not observed in the sinusoidal ripples where the DOS remains similar to that of unstrained graphene (black line).

5. Conclusions

The use of a state-of-the-art empirical force field in atomistic modelling of covalently bonded materials was tested for the 2D crystal graphene. Despite the fact that the potential is deliberately designed to replicate the properties of 3D C-Diamond, the accurate physical description of the atomic interactions is entirely transferred to the 2D case of graphene. We have used the MMP force field to calculate both vibrational properties and performing molecular dynamics of ripple formation.

The calculation of phonon dispersions and bandstructure was used here for two external strain combinations. Though direct modelling of Raman spectra would go beyond the scope of this work, the method presented here clearly provides a route to do so and hence extract quantitative information directly from spectroscopic results on graphene.

The molecular dynamics simulation of graphene have highlighted two major types of ripples: wave front and sinusoidal. We support examples and strain patterns of both types of ripples by Transmission Electron Microscopy.

Ripples appear to arise in the presence of compressive strain in a single direction orthogonal to the wave front, or hydrostatic compression for the sinusoidal type. This suggests that manipulating strain on the surface of graphene can lead to control of the type of generated ripple.

The wavefront ripple leads to an appreciable bandgap opening of 0.22 eV and a simultaneous detectable change in the phonon dispersion.

The sinusoidal case presents the most interesting strain pattern. Tensile and compressive strain is found on the opposite sides of the V-shape. Compressive and tensile strain results in opposite types of bandstructures. The tensile strain region is the only one that exhibits a bandgap opening of around 0.19 eV (Fig. 3(A and B)), whereas the compressive region shows spontaneous n-doping characteristics (Fig. 3(D and E)). The surface of graphene therefore results in a sequence of doped and undoped semiconducting/metallic regions of nanoscale dimension, in close proximity to each other, and obtainable on demand by application of hydrostatic compression. Our experimental electron microscopy shows how e.g. hydrocarbon impurities can produce the required strain and therefore could be exploited to design desired strain patterns.

The predicted link between strain, bandgap opening and phonon frequencies provides a new possibility for exploitation of graphene as an electronic material by virtue of control of the metallic/semiconducting transport characteristic in proximity of the ripples.

Furthermore, inducing controllable strain on a graphene sheet, by means of processing contaminants or deposition of regular metallic patterns, could generate ripples with

n-doped regions. This can be exploited to support current generation as a result of externally applied mechanical deformation, which could lead to the realisation of graphene based pressure sensor or nanoelectromechanical machines like nanogenerators.

6. Methods

The parameterization and validation of the MMP potential [24,25] for diamond and graphene was performed using in house software, comprising a true random number generator based parameter search routine and using the dynamical matrix approach with analytic first and second order derivatives of the force field for the calculation of phonon dispersions. The molecular dynamics was performed on an ad hoc modified version of the IMD™ software [50]. The simulations start with a flat graphene sheet with a lattice constant expanded or reduced by a certain amount of strain and all the atoms are allowed to move along the three coordinate axes. We applied periodic boundary conditions on the *xy* plane only and no initial velocity or pressure is applied to stimulate or control the out-of-plane motions. A constant volume, constant energy ensemble integrator, starting from a zero temperature with 0.005 time step was used.

The experimental data was collected using an advanced transmission electron microscope with very precise control over the focus by variations of the crispness of high resolution lattice images. If the top of a ripple is in focus, the flanks and troughs will be increasingly out-of-focus. Such difference manifests itself in contrast changes. We make use of atomic resolution images obtained in a JEOL ARM200F FEG-STEM/TEM microscope, equipped with CEOS hexapole probe and image corrector operating at 80 kV and a Gatan SC1000 ORIUS™ CCD camera and high angle annular dark field (HAADF), obtained either in a probe and image corrected Jeol ARM transmission electron microscope, a dedicated probe corrected scanning transmission electron microscope (STEM) or a Nion UltraSTEM (for an example see Fig. S2).

Bandstructure calculations were performed using the nextnano software [51]. We modified the Tight Binding routine to generalise to both a 2×2 strain tensor but also for the presence of internal displacement. We used the general Tight Binding implementation that includes 3rd nearest neighbours, together with the parameters credited to R. Scholtz (currently at the Technical University of Dresden).

Author contributions

The modelling work was performed by authors U. Monteverde, J. Pal, M.A. Migliorato. The graphics in Figs. 3 and 4 were created by U. Monteverde. D. Powell contributed to the code development and is credited with laying the foundations for the present development of the MMP potential. R. Zan provided and screened the graphene samples, R. Kashtiban obtained the HREM images and U. Bangert carried out the electron microscopy analysis. M.A. Migliorato and M. Missous compiled the article with input from the other authors.

Competing financial interests

Patent application number GB1406788.8.

Acknowledgements

We are indebted to Dr. Stephan Birner of nextnano GmbH for his help with the modification needed of the Tight Binding routines in the nextnano source code. We are also grateful to Prof S. Clark of Durham University (UK) and Prof R.J. Young FRS (University of Manchester) for valuable discussions. We like to thank the UK Engineering and Physical Sciences Research Council (EPSRC) for Doctoral Prize Fellowship. We would also like to acknowledge Dr. Brian May CBE, of the band Queen, for kindly granting us permission to use the song *Under Pressure* (Queen and David Bowie, 1981) as soundtrack for our molecular dynamics video (Video S1). Due to copyright reasons the song was not used.

Appendix A. Supplementary data

Supplementary data associated with this article can be found, in the online version, at http://dx.doi.org/10.1016/j.carbon.2015.04.044.

REFERENCES

[1] Schaible M. Empirical molecular dynamics modeling of silicon and silicon dioxide: a review. Crit Rev Solid State Mater Sci 1999;24:265–323.
[2] Tersoff J. New empirical approach for the structure and energy of covalent systems. Phys Rev B 1988;37:6991–7000.
[3] Powell D, Migliorato MA, Cullis AG. Optimized Tersoff potential parameters for tetrahedrally bonded III–V semiconductors. Phys Rev B 2007;75:115202-1–9.
[4] Los JH, Fasolino A. Intrinsic long-range bond-order potential for carbon: performance in Monte Carlo simulations of graphitization. Phys Rev B 2003;68:024107-1–024107-14.
[5] Stuart SJ, Tutein AB, Harrison JA. A reactive potential for hydrocarbons with intermolecular interactions. J Chem Phys 2000;112:6472–86.
[6] Los JH, Ghiringhelli LM, Meijer EJ, Fasolino A. Improved long-range reactive bond-order potential for carbon. I. Construction. Phys Rev B 2005;72:214102-1–214102-14.
[7] Tewary VK, Yang B. Parametric interatomic potential for graphene. Phys Rev B 2009;79:075442-1–9.
[8] Brenner DW, Shenderova OA, Harrison JA, Stuart SJ, Ni B, Sinnott SD. A second-generation reactive empirical bond order (REBO) potential energy expression for hydrocarbons. J Phys Condens Matter 2002;14:783–802.
[9] Lindsay L, Broido DA. Optimized Tersoff and Brenner empirical potential parameters for lattice dynamics and phonon thermal transport in carbon nanotubes and graphene. Phys Rev B 2010;81:205441-1–6.
[10] Ru CQ. Ripple formation of free graphene ribbons driven by self-attractive forces. Appl Phys Lett 2013;103:043104.
[11] Karssemeijer LJ, Fasolino A. Phonons of graphene and graphitic materials derived from the empirical potential LCBOPII. Surf Sci 2011;605:1611–5.
[12] Novoselov KS. Two-dimensional gas of massless Dirac fermions in graphene. Nature 2005;438:197–200.

[13] Meyer JC, Geim AK, Katsnelson MI, Novoselov KS, Booth TJ, Roth S. The structure of suspended graphene sheets. Nature 2006;446:60–3.
[14] Fasolino A, Los JH, Katsnelson MI. Intrinsic ripples in graphene. Nat Mater 2007;6:858–61.
[15] Wang WL, Bhandari S, Yi W, Bell DC, Westervelt R, Kaxiras E. Direct imaging of atomic-scale ripples in few-layer graphene. Nano Lett 2012;12:2278–82.
[16] Thompson-Flagg RC, Mouraand MJB, Marder M. Rippling of graphene. EPL 2009;85:46002-1–4.
[17] Sun GF, Jia JF, Xue QK, Li L. Atomic-scale imaging and manipulation of ridges on epitaxial graphene on 6H-SiC(0001). Nanotechnology 2009;20:355701-1–4.
[18] Zhu W, Low T, Perebeinos V, Bol AA, Zhu Y, Yan H, et al. Structure and electronic transport in graphene wrinkles. Nano Lett 2012;12:3431–6.
[19] Miranda R, Vázquez de Parga AL. Graphene: surfing ripples towards new devices. Nat Nanotechnol 2009;4:549–50.
[20] Santos EJG, Riikonen S, Sánchez-Portal D, Ayuela A. Magnetism of single vacancies in rippled graphene. J Phys Chem C 2012;116:7602–6.
[21] Naumov II, Bratkovsky M. Gap opening in graphene by simple periodic inhomogeneous strain. Phys Rev B 2011;84:245444-1–6.
[22] Bao W, Miao F, Chen Z, Zhang H, Jang W, Dames C, et al. Controlled ripple texturing of suspended graphene and ultrathin graphite membranes. Nat Nanotechnol 2009;4:562–6.
[23] Wang Y, Yang R, Shi Z, Zhang L, Shi D, Wang E, et al. Super-elastic graphene ripples for flexible strain sensors. ACS Nano 2011;5:3645–50.
[24] Monteverde U, Migliorato MA, Pal J, Powell D. Elastic and vibrational properties of group IV semiconductors in empirical potential modelling. J Phys Condens Matter 2013;25:425801-1–425801-10.
[25] Monteverde U, Migliorato MA, Powell D. Empirical interatomic potential for the mechanical, vibrational and thermodynamic properties of semiconductors. J Phys Conf Ser 2012;367:012015-1–5.
[26] Porter LJ, Justo JF, Yip S. The importance of Grüneisen parameters in developing interatomic potentials. J Appl Phys 1997;82:5378–81.
[27] Madelung O, Schulz M, Weiss H. Intrinsic properties of group IV elements, III–V, II–VI and I–VII compounds. Berlin: Springer; 1987.
[28] Warren JL, Yarnell JL, Dolling G, Cowley AR. Lattice dynamics of diamond. Phys Rev 1967;158:805–8.
[29] Schwoerer-Böhning M, Macrander AT. Phonon dispersion of diamond measured by inelastic X-ray scattering. Phys Rev Lett 1998;80:5572–5.
[30] Burkel E. Determination of phonon dispersion curves by means of inelastic X-ray scattering. J Phys Condens Matter 2001;13:7627–44.
[31] Kulda J, Kainzmaier H, Strauch D, Dorner B, Lorenzen M, Krisch M. Overbending of the longitudinal optical phonon branch in diamond as evidenced by inelastic neutron and X-ray scattering. Phys Rev B 2002;66:241202.
[32] Windl W, Pavone P, Karch K, Schütt O, Strauch D, Giannozzi P, et al. Second-order Raman spectra of diamond from ab initio phonon calculations. Phys Rev B 1993;48:3164–70.
[33] Mohr M, Maultzsch J, Dobardžić E, Reich S, Milošević I, Damnjanović M, et al. Phonon dispersion of graphite by inelastic x-ray scattering. Phys Rev B. 2007;76:035439-1–7.
[34] Wirtz L, Rubio A. The phonon dispersion of graphite revisited. Solid State Commun 2004;131:141–52.
[35] Zan R, Muryn C, Bangert U, Mattocks P, Wincott V, Vaughan D, et al. Scanning tunnelling microscopy of suspended graphene. Nanoscale 2012;4:3065–8.
[36] Korznikova EA, Dmitriev SV. Moving wrinklon in graphene nanoribbons. J Phys D Appl Phys 2014;47:345307.
[37] Baimova JA, Dmitriev SV, Zhou K, Savin AV. Unidirectional ripples in strained graphene nanoribbons with clamped edges at zero and finite temperatures. Phys Rev B 2012;86:035427.
[38] Dong Y, He Y, Wang Y, Li H. A theoretical study of ripple propagation in defective graphene. Carbon 2014;68:742–7.
[39] Breitwieser R, Hu YC, Chao YC, Li RJ, Tzeng YR, Li LJ, et al. Flipping nanoscale ripples of free-standing graphene using a scanning tunneling microscope tip. Carbon 2014;77:236–43.
[40] Yu T, Ni Z, Du C, You Y, Wang Y, Shen Z. Raman mapping investigation of graphene on transparent flexible substrate: the strain effect. J Phys Chem C 2008;112:12602–5.
[41] Ferrari AC, Basko DM. Raman spectroscopy as a versatile tool for studying the properties of graphene. Nat Nanotechnol 2013;8(4):235–46.
[42] Davydov YS. On the elastic characteristics of graphene and silicene. Phys Solid State 2010;52:184–7.
[43] Young RJ, Gong L, Kinloch IA, Riaz I, Jalil R, Novoselov KS. Strain mapping in a graphene monolayer nanocomposite. ACS Nano 2011;5:3079–84.
[44] Bangert U, Gass MH, Bleloch AL, Nair RR, Geim AK. Manifestation of ripples in free-standing graphene in lattice images obtained in an aberration-corrected scanning transmission electron microscope. Phys Status Solidi A 2009;206:1117–22.
[45] Guinea F, Katsnelson MI, Geim AK. Energy gaps and a zero-field quantum Hall effect in graphene by strain engineering. Nat Phys 2010;6:30–3.
[46] Gui G, Li J, Zhong J. Band structure engineering of graphene by strain: first-principles calculations. Phys Rev B 2008;78:075435.
[47] Zhou SY, Gweon GH, Fedorov AV, First PN, de Heer WA, Lee DH, et al. Substrate-induced bandgap opening in epitaxial graphene. Nat Mater 2007;6:770–5.
[48] Rotenberg E. Origin of the energy bandgap in epitaxial graphene. Nat Mater 2008;7:258–9.
[49] Balog R, Jørgensen B, Nilsson L, Andersen M, Rienks E, Bianchi M, et al. Bandgap opening in graphene induced by patterned hydrogen adsorption. Nat Mater 2010;9:315–9.
[50] Stadler J, Mikulla R, Trebin HR. IMD: a software package for molecular dynamics studies on parallel computers. Int J Mod Phys C 1997;8:1131–40.
[51] Birner S, Zibold T, Andlauer T, Kubis T, Sabathil M, Trellakis A, et al. Nextnano: general purpose 3-D simulations. IEEE Trans Electron Devices 2007;54:2137–42.